THE JOURNAL OF PHYSICAL CHEMISTRY B

Article

pubs.acs.org/JPCB

Nanoparticle Growth Analysis by Molecular Dynamics: Cubic Seed

Donguk Suh and Kenji Yasuoka*

Department of Mechanical Engineering, Keio University, 3-14-1 Hiyoshi, Kohokuku, Yokohama 223-8522, Japan

ABSTRACT: Growth of a cubic nanoparticle was studied by classical molecular dynamics simulation for three seed sizes in nine different supersaturation ratios. Similar to the spherical seed in our previous study, for high supersaturation ratios, a two-stage phenomenon that consists of an initial heterogeneous growth around the seed and homogeneous nucleation at various sites within the system was observed. A decomposition of the distinct phenomenon was carried out and the results were compared to that from the spherical seed. The homogeneous nucleation characteristics for high supersaturation ratios show no significant difference, but as the supersaturation ratio decreases, the ratio of the nucleation rate for the systems with different seed shapes shows a deviation from unity. Other tendencies are nearly identical to that seen from the spherical seed study and the physical rationales are alike. The heterogeneous growth rate was greater by a factor of 3 to 10, even though the number of molecules in each seed class was nearly identical, which is evidence of a shape effect. Furthermore, cluster formation free energy analysis was conducted and the results were compared with the classical nucleation theory and condensation theory. The disk-shape modification of the classical nucleation theory was used for growth on the cubic seed and produced a similar deviation to that of the spherical seed, which used a cap-shape modification. Additionally, the condensation theory showed a better agreement compared with the sphere. Finally, the nanoparticle growth mechanism on the seeds along with the packing and surface diffusion characteristics was analyzed and showed why and how the nanoparticle grows.

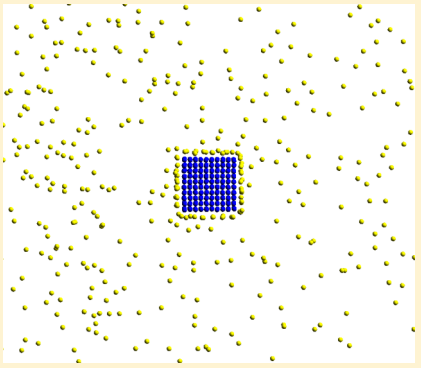

1. INTRODUCTION

Nanoparticle growth based on heterogeneous nucleation of vapor condensing on solid seeds is a phenomenon associated with applications in various fields such as cosmology, meteorology, environmental engineering, mechanical engineering, and material engineering.[1−7] Numerous theoretical studies exist, but they mainly focus on the precursor particles having a spherical configuration.[8−13] This is because a sphere is a unique configuration that has known mathematical solutions. In nature, if the precursor particle is liquid, it is typically spherical because of surface tension. Hence, barring external forces, droplets are spherical, and growth occurs isotropically. To the contrary, crystal growth is nonisotropic (orientation-dependent) and, based on the Berg Effect, can be favorable on vertices and edges.[14−17] Therefore, in reality, nanoscale solid seed particles in nature are very rarely complete spheres and normally have flat faces and edges. Though there have been experimental studies that compare their findings on growth characteristics with theoretical studies, the comparisons are relatively indirect because the precursor particles have edges, whereas the theoretical values are based on spherical particles.[18] Therefore, confirming whether the rate of growth on nanoparticles is affected by the edges becomes an interesting problem. Moreover, if edge effects do exist, the degree of the influence is the next obvious question.

To study the growth on a nanoscale seed particle, molecular dynamics (MD) was the simulation method of choice because the phenomenon can be directly analyzed microscopically. There have been some studies by MD on heterogeneous growth on precursor particles, but none have studied growth on cubic seeds or particles that have distinct edges. Matsubara et al.[19] studied nucleation of water occurring on sulfuric acid molecules, and focused on how concentration of the sulfuric acid and coagulation of hydrates increases the amount of nucleation. Walsh et al.[20] conducted a lengthy simulation on the formation of methane clathrates and confirmed that classical MD can be used for clathrate hydrate studies by being able to actually visualize the generation process of the cage structure of the hydrates. Water condensing on large organic molecules was also investigated by Darvas et al.,[21] where the phase diagram of the binary mixture was produced. Inci and Bowles[22] studied the growth of a film on a spherical insoluble seed particle and compared the simulation results, with the classical nucleation theory (CNT) finding good agreement. Suh and Yasuoka,[23] which is a prequel to this study, also examined condensation on a spherical particle and found nucleation to occur in two stages and the heterogeneous growth to be independent of the supersaturation ratio unlike CNT. The existence of condensation studies on specific molecules like sulfuric acid and methane renders the understanding on how heterogeneous nucleation occurs on fundamental geometrical configurations such as a sphere, and so the next shape of interest is naturally a cube. In reality, many solid particles such as ionic bonding substances like NaCl or

Received: May 8, 2012
Revised: October 31, 2012
Published: November 7, 2012

dx.doi.org/10.1021/jp3044658 | J. Phys. Chem. B 2012, 116, 14637−14649

metals have lattice structures, where some may result in a cube.[24,25]

The biggest difference between a sphere and a cube lies in the existence of edges, and therefore, whether the condensation will be affected by the edges on a cubic seed particle becomes a prominent question. There are actually many experimental studies on how the edge affects growth of crystals and construction of thin films.[26−29] The studies found the edges to present different morphological growth characteristics compared to the surfaces. The rate of the growth, however, is yet to be clarified, and therefore, this study aims to provide an answer.

As stated, this is a sequel to the study on nanoparticle growth for spherical seed particles,[23] so most of the methodologies that have been applied are the same. The main difference is the shape of the seed placed inside the system. The nucleation and growth rates were calculated from decomposed cluster size distribution plots by the Yasuoka-Matsumoto (YM) method.[30] The ensuing section will briefly review the analysis methods along with new methods used to analyze the cubic configuration. Thereafter, the simulation setup will be presented, which will be followed by the results of this study.

2. ANALYSIS METHODS

Kinetic analysis, cluster formation free energy analysis, condensation theory, and CNT were the analysis methods. Besides CNT, the other three methods are exactly the same as was used in the previous study.[23] Hence, this section will simply summarize the other methods, and focus more on explaining how the growth rate on a cubic seed is calculated for the classical nucleation theory.

2.1. Kinetic Analysis. This method is used to observe the attachment and detachment behavior of molecules onto n-sized clusters.[30,31] The transition probability β for a certain time Δt (10.0 ps) of an n-mer to an $(n+k)$-mer during nucleation can be calculated by eq 1. The denominator is the time average of $M_{n,n+k}(t)$, which is the number of size change events at a certain duration of time, and the numerator is the sum for all cluster sizes. The forward and backward rates are each calculated from eqs 2 and 3.

$$\beta_{n,n+k} = \frac{\langle M_{n,n+k}(t)\rangle_t}{\sum_{k=-\infty}^{\infty}\langle M_{n,n+k}(t)\rangle_t} \tag{1}$$

$$\langle k\rangle_+(n) = \sum_{k=1}^{\infty} k\beta_{n,n+k} \tag{2}$$

$$\langle k\rangle_-(n) = \sum_{k=-\infty}^{-1} k\beta_{n,n+k} \tag{3}$$

2.2. Cluster Formation Free Energy Analysis. Though the YM method provides the overall nucleation rate, it does not give any information about the free energy barrier. Therefore, this analysis method is essential when comparing the results with CNT because it acts as a bridge in the understanding of the simulation and theoretical results. The cluster formation free energy $\Delta G(n)$ of an n-mer (eq 4) is calculated from the equilibrium number density $\rho_{eq}(n)$ in eq 5.[30−32] The simulation results directly produce the steady state number density $\rho_{ss}(n)$ and nucleation rate J_{MD}. Moreover, $B(n)$ is found from eqs 2 and 3, whereas k_B is the Boltzmann constant, and T is the system temperature.

$$\Delta G(n) = -k_B T \ln[\rho_{eq}(n)/\rho_{eq}(1)] \tag{4}$$

$$\rho_{eq}(n) = \rho_{ss}(n)\exp\left[J_{MD}\sum_{i=1}^{n}\frac{1}{B(i)\rho_{ss}(i)}\right] \tag{5}$$

$$B(n) = \frac{\langle k\rangle_+(n) - \langle k\rangle_-(n)}{2} \tag{6}$$

2.3. Condensation Theory. The condensation rate J_{Con} is calculated by eq 7.[33] $f(\mathrm{Kn})$ is a correction factor, where Kn is the Knudsen number, λ is the mean free path, P is the supersaturated vapor pressure, and D_{Ar} is the molecular diameter for argon (3.84 Å). Additionally, D_p is the characteristic length for the wetted particle, which is equivalent to $(3l)^{1/2}$, where l is the edge length of the cube.

$$J_{Con} = \rho_v(S-1)\sqrt{\frac{k_B T}{2\pi m}}f(\mathrm{Kn}) \tag{7}$$

$$f(\mathrm{Kn}) = \left(\frac{1.333\mathrm{Kn} + 1.333\mathrm{Kn}^2}{1 + 1.71\mathrm{Kn} + 1.333\mathrm{Kn}^2}\right) \tag{8}$$

$$\mathrm{Kn} = 2\lambda/D_p \tag{9}$$

$$\lambda = \frac{k_B T}{\pi D_{Ar}^2\sqrt{2}\,P} \tag{10}$$

2.4. Classical Nucleation Theory. As was for the spherical seed, condensation on a cubic seed also starts from complete wetting (Figure 1), so the growth cannot be characterized as a cap-shape on a sphere, which was the model used by Fletcher.[34] According to Kashchiev,[35] the growth model should take the form of a "disk-shape", because the seed surface is overly wetted and thus creates a monolayer that can be called an "own substrate." Eq 11 is one form of the Gibbs free energy, where n is the number of molecules, $\Delta\mu$ is the chemical potential difference between the old and new phase during the

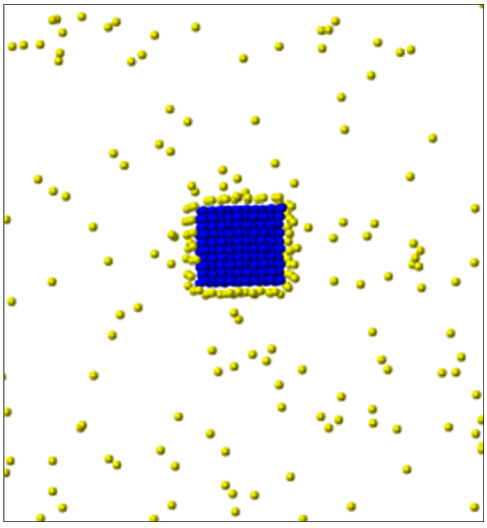

Figure 1. Magnified slice plot (thickness 4.0) of a completely wetted seed at the onset of nucleation. Blue dots in the center are the molecules within the cubic seed, whereas the yellow is the vapor molecules.

dx.doi.org/10.1021/jp3044658 | J. Phys. Chem. B 2012, 116, 14637−14649

nucleation process, b is a shape factor, and κ is the specific line energy of the cluster growing on the substrate.

$$G(n) = -n\Delta\mu + b\kappa n^{1/2} \tag{11}$$

$$\Delta\mu = k_B T \ln S \tag{12}$$

$$b = 4(v_l/d_0)^{1/2} \tag{13}$$

$$\kappa = \gamma d_0 \tag{14}$$

Equation 12 is a common approximation for vapor condensation, where S is the supersaturation ratio. The supersaturation ratio in this study is a partial molar property solely of the target vapor. The shape factor in eq 13 is for a square-shaped disk, and just for reference, a circular disk is $2(\pi v_l/d_0)^{1/2}$. v_l and d_0 are the specific liquid volume and monolayer thickness, respectively. The specific line energy (eq 14) can also be represented by the monolayer thickness multiplied by the surface tension γ. Therefore, for a square-shaped disk growing on an insoluble substrate, eq 11 takes the form of eq 15. The critical nucleus size n^* can be calculated through the extremum of eq 15, which becomes eq 16.

$$\Delta G(n) = -n\Delta\mu + 4\gamma(v_l d_0 n)^{1/2} \tag{15}$$

$$n^* = \frac{4\gamma^2 v_l d_0}{\Delta\mu^2} \tag{16}$$

For completeness, in the case of homogeneous nucleation, the following equations are used.

$$\Delta G^* = \frac{16\pi v_l^2 \gamma^3}{3(k_B T \ln S)^2} \tag{17}$$

$$n^* = \frac{32\pi v_l^2 \gamma^3}{3(k_B T \ln S)^3} \tag{18}$$

The nucleation rate J is defined as the number of nuclei per volume per time for homogeneous nucleation. Likewise, the growth rate is also denoted by J and is defined as the number of molecules that attach to the surface of the initial wetted particle per surface area of the initial particle per time. The homogeneous nucleation rate and growth rate can both be presented by the following equation:

$$J = zf^* C_0 \exp[-\Delta G(n^*)/k_B T] \tag{19}$$

where z, f^*, and C_0 are the Zeldovich factor, forward rate, and concentration of sites, respectively. When calculating the homogeneous nucleation rate, eq 17 is plugged into eq 19, whereas eq 15 is used to calculate the growth rate. The Zeldovich factor can be calculated by extracting the double derivative of the free energy barrier in eq 20 by curve fitting eq 4 or using an approximated value in eq 21.[36]

$$z = \sqrt{\frac{-1}{2\pi k_B T} \cdot \left.\frac{\partial^2 \Delta G(n)}{\partial n^2}\right|_{n=n^*}} \tag{20}$$

$$z = \sqrt{\frac{\ln S}{6\pi n^*}} \tag{21}$$

f^* is determined by eq 22 or directly found through eq 2 by calculating n^*. ρ_v is the number density of monomers, while m is the mass of a monomer. $C_0 = \rho_v$ is typically used for homogeneous nucleation,[30,31] and eq 23 was used for the heterogeneous case.

$$f^* = \sqrt{\frac{k_B T}{2\pi m}} \rho_v (6\sqrt{\pi} v_l n^*)^{2/3} \tag{22}$$

$$C_0 = \frac{n^{*2/3}}{6l^2} \tag{23}$$

3. SIMULATION SETUP

The dimensions of the seeds for the sphere and cube are presented in Table 1. All length dimensions are non-dimensionalized by the aluminum molecular length σ_{Al} = 2.551 Å. There are three seed sizes, which is the number of molecules inside the seed for each seed type, and the slight difference of the seed sizes between the seed types for the sphere originates from the construction method.[23] A seed was initially constructed by cutting out a bulk of aluminum having a face-centered-cubic lattice equilibrated by the embedded atom method[37] with a density of 2700 kg/m^3, but the spherical cutting of a cubic lattice could not produce the exact number of seeds as the cube, and thus, the slight difference in the number of molecules for the shapes exist. As in the spherical case, vibration or a breathing mode[38,39] of the seed particle was observed, so the dimensions are time averages of the lengths of the seeds. Target and carrier molecules were equilibrated at an initial density fixed to 100.0 kg/m^3 and every molecule was a Lennard-Jones particle. The target and carrier atoms both had argon properties σ_{Ar} = 3.405 Å for the molecular length and 1.67×10^{-21} J (119.8 K) for the potential well depth, but the latter only had repulsive interactions as in the previous study for a spherical seed.[23] The seed molecules were aluminum,[40] where the potential well depth was 0.65×10^{-19} J (4663 K). There were 21952 argon-like molecules and, among them, 10000 were carrier molecules, and the addition of the number of seed molecules in Table 1 gives the total number of molecules within a system.

Table 1. Initial Dimensions of the Seed Particle in Dimensionless Units by the Aluminum Molecular Length σ_{Al}[a]

seed type	seed size	diameter (σ_{Al})	surface area (σ_{Al}^2)
sphere	110	5.644	100.0
	255	7.727	187.5
	502	9.563	287.1
	seed size	edge (σ_{Al})	surface area (σ_{Al}^2)
cube	108	3.651	79.97
	256	5.189	161.6
	500	6.732	272.0

[a]Seed size refers to the number of molecules within the seed per each system. The smallest to the largest cubic seeds had 3, 4, and 5 unit cells.

To produce an initial system, a seed particle was placed inside a cubic periodic box with a simple cubic block of argon-like molecules for equilibration. The initial equilibration temperature was 241.38 K for 0.8 ns and another 0.2 ns was carried out without velocity rescaling for relaxation. During the entire equilibration time of 1.0 ns, all of the vapor molecules only had repulsive interactions. Furthermore, although there

dx.doi.org/10.1021/jp3044658 | J. Phys. Chem. B 2012, 116, 14637−14649

Table 2. Summary of the Supersaturation Ratio Variation, ΔS, for Systems with Each Seed Type over All Replications, Calculated as $\Delta S = (\Sigma S_{avg}/3 - S_{init})/S_{init}$[a]

	S_{avg}			ΔS		
	seed size			seed shape		$\frac{\Delta S_{cube} - \Delta S_{sphere}}{\Delta S_{sphere}} \times 100$
S_{init}	108	256	500	cube	sphere	%
10.23	8.82	8.81	8.78	−0.140	−0.142	−1.73
9.25	8.17	8.16	8.13	−0.119	−0.121	−1.72
8.12	7.32	7.24	7.27	−0.104	−0.103	1.56
7.15	6.54	6.49	6.50	−0.0891	−0.0908	−1.86
6.17	5.68	5.65	5.65	−0.0825	−0.0844	−2.22
5.11	4.75	4.73	4.72	−0.0738	−0.0760	−2.93
4.27	3.99	3.98	3.97	−0.0683	−0.0694	−1.55
3.04	2.87	2.87	2.84	−0.0586	−0.0596	−1.73
2.22	2.11	2.11	2.10	−0.0511	−0.0538	−5.15

[a]The three S_{avg} values that are summed are the average supersaturation ratios for each seed size over all five replications for the cubic seed.

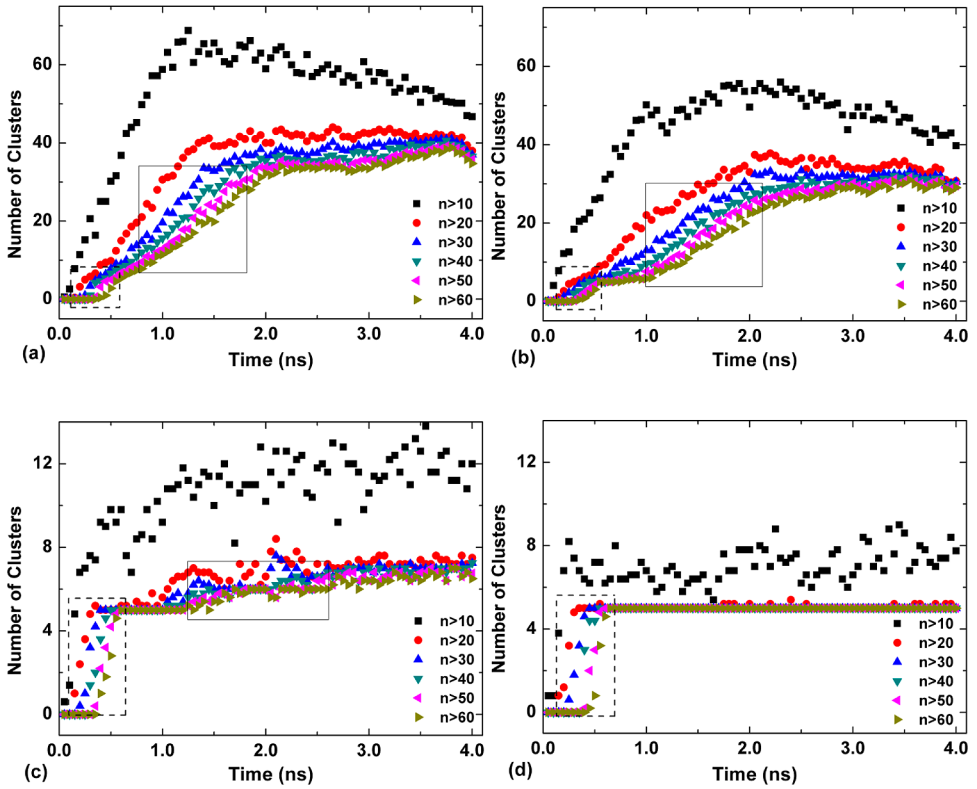

Figure 2. Number of clusters plotted for seed size 108. (a) S = 10.23, (b) 9.25, (c) 6.17, and (d) 5.11. The dashed rectangle outlines growth on the seed, whereas the solid rectangle shows homogeneous nucleation.

was no attraction for the vapor molecules, some of the molecules could be seen attaching onto the seed surface.

The system has three different system volumes because the numbers of seed atoms vary. The length of one side is 95.9, 96.1, and 96.4 for the smallest to the largest seed sizes, respectively. The target−seed and seed−seed interactions are basically LJ interactions that use the Lorentz−Berthelot relations, as in ref 23, and velocity rescaling was used on the carrier molecules to control the system temperature. Additionally, time integration was performed by the leapfrog Verlet algorithm, and a time step of 5.0 fs and a cutoff radius of 4.5 σ_{Al} was used throughout the entire simulation.[30,41−43] Nine supersaturation ratios, 2.22, 3.04, 4.27, 5.11, 6.17, 7.15, 8.12, 9.25, and 10.23, were evaluated, where the S values correspond to 114.96, 109.8, 104.64, 102.06, 99.48, 97.6, 96.00, 94.32, and 93.20 K, respectively.[44] Moreover, five replications were conducted for each seed type. To obtain better statistics for the nucleation and growth rates, the data from the five replications were merged into one in order to apply the YM method.[30] Details of the YM method and the rationale to its use are thoroughly explained in Suh and Yasuoka.[23] In addition, a Stillinger radius of 1.5 σ_{Al} is used to define a cluster.[40,45]

Figure 1 is a magnification of the seed, where instantaneous complete wetting occurs for all cases right after the initiation of nucleation. A monolayer has grown on the seed surface and will be further analyzed later in the text.

dx.doi.org/10.1021/jp3044658 | J. Phys. Chem. B 2012, 116, 14637−14649

The aforementioned nine Ss are initial values at the onset of nucleation (denoted as S_{init}). The supersaturation ratio subsides during the simulation process because an *NVT* ensemble is used. The summary of ΔS, which measures the S decrease from S_{init}, is in Table 2, and the average of S during the nucleation period (between 0.5 to 2.0 ns) for each seed type is S_{avg}, where all replications are included. A steady state is assumed during the nucleation period despite a relatively large ΔS at high supersaturation ratios because the S variation is considered to be insignificant within the nucleation period. By comparing ΔS of the spherical and cubic seed, one can see that the former is generally slightly greater than the latter, but there is no clear evidence that this difference affects nucleation. Moreover, a critical S value (within the observed time frame of 4.0 ns) between 5.11 and 6.17 has been found from previous studies on homogeneous systems.[46]

4. RESULTS

The two-stage phenomena, which was seen in the spherical case can also be seen for the cubic seed. One big difference is that for the spherical seed at the highest S, heterogeneous growth could not be seen,[23] but for the cube, a distinct growth on the seed is observable as in Figure 2.

A decomposition of the combined homogeneous and heterogeneous phenomena was performed again and plotted in Figure 3. The decomposition method is very straightforward, where one initially creates the cluster distribution plot as in Figure 2. The next step is to create the same plot just for the seeds as in Figure 3b. Finally, the decoupled homogeneous plot (Figure 3a) can be extracted by simply subtracting the seed data from the original data (Figure 2a). The nucleation and growth rates were calculated by dividing the slopes of the distributions by the system volume and initial surface area, respectively.

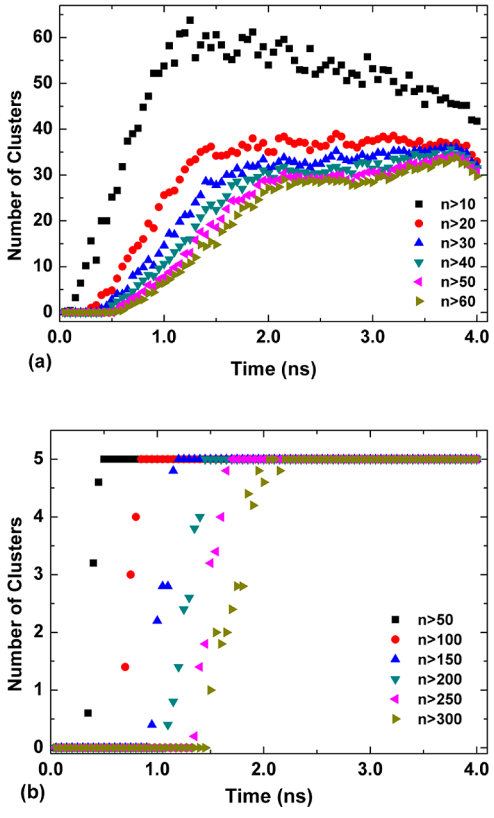

Figure 3. Plot for number of clusters for seed size 108 at S = 10.23, where the plots are a decomposition of Figure 2a: (a) homogeneous part and (b) heterogeneous part.

4.1. Homogeneous Nucleation. The homogeneous nucleation rates exist only above the aforementioned critical supersaturation ratio. The resulting values are depicted in Figure 4 against the supersaturation ratio. No clear seed size

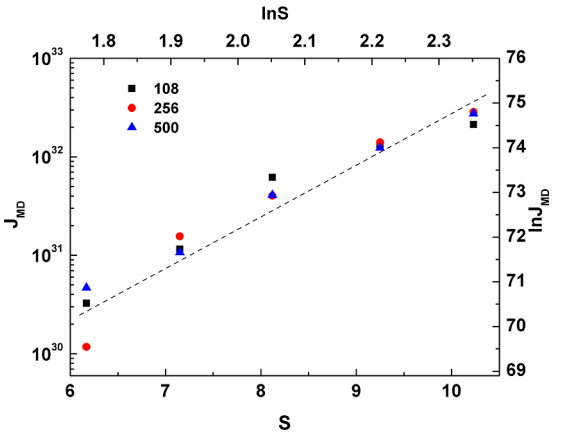

Figure 4. Homogeneous nucleation rate plot for all cubic seed sizes from the simulation data. The dashed line is the linear fit for all the data points based on the right and top axes. The slope is 8.877, which can be translated to a critical nucleus size of 7.877.

dependence can be seen for all S values. According to Kashchiev,[47] by eq 24 the slope of the natural log values can be converted to the critical nucleus size, which is found to be 7.877. The homogeneous system for the sphere had a size of 5.698, which means that nucleation occurs more easily for the system with a spherical seed.

$$n^* = \frac{\partial \ln J}{\partial \ln S} - 1 \tag{24}$$

The comparison for the nucleation rate between the two shapes in Figure 5 show that at high supersaturation ratios, there is an insignificant difference, but as S decreases, the seed particle becomes more influential, and the system with the spherical seed has a higher nucleation rate. This is a clue that there are less monomers for the cubic seed because there is

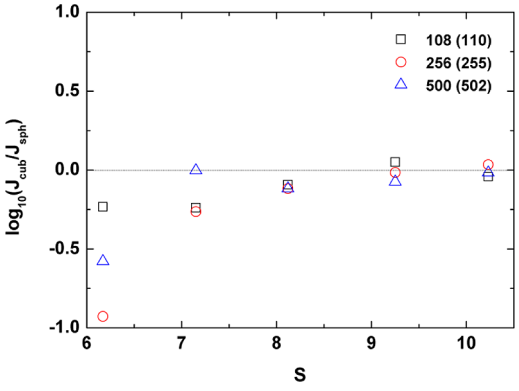

Figure 5. Homogeneous nucleation rate comparison between the cubic and spherical seed from MD. The homogeneous nucleation rates show little deviation from each other for high supersaturation ratios, but there is less nucleation for the cubic seed at lower S values, which signifies the seed influencing homogeneous nucleation.

dx.doi.org/10.1021/jp3044658 | J. Phys. Chem. B 2012, 116, 14637−14649

more growth on the cubic seed, which makes the nucleation rate for the sphere faster. Therefore, we can conclude that the seed size or shape does not influence homogeneous nucleation characteristics for high supersaturation ratios, which is physically comprehensible because nucleation of clusters around the seed should not be affected by the seed. But at low supersaturation ratios, the seed manipulates homogeneous nucleation through the supersaturation ratio.

Figure 6a is a comparison of homogeneous nucleation rates of CNT with MD, whereas Figure 6b is that of the cluster

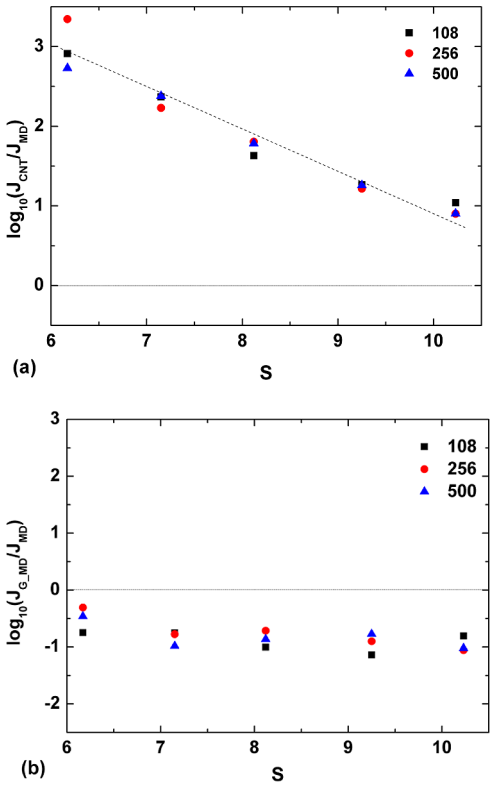

Figure 6. (a) CNT and MD comparison for the homogeneous nucleation rate. (b) Cluster formation free energy method and MD comparison for the nucleation rate.

formation free energy with the simulation results. The nucleation rate from CNT was calculated by eqs 17 and 19, where the thermodynamic forward rate, Zeldovich factor, and number of concentration sites, are from Table 3, Table 4, and the monomer number density, respectively. The specific liquid volume for small clusters was found from Thompson et al.,[48] and the surface tension was computed by using the results from Chapela et al.[49] For the CNT comparison in Figure 6a, two aspects are distinct, where one is the 1−3 order discrepancy and the other is the declining trend. The overall trend is similar to not only the data from the spherical seed[23] and other MD results,[31,50] but also experimental studies.[51,52]

The nucleation rate from the cluster formation free energy in Figure 6b was also obtained by using eq 19. The sole difference for input values was in the exponential term, which was calculated by the cluster formation free energy method in section 2.2. The nucleation rate extracted by MD is about an order higher than that estimated by the cluster formation free energy method, but the tendencies coincide over the observed supersaturation ratio range. By comparing the results from the cluster formation free energy method (eq 4) and CNT (eq 17)

Table 3. Forward Rate f^* from Kinetic Analysis and the Thermodynamic Approximation[a]

		$f^*(s^{-1})$	
S	seed type	kinetic	thermodynamic
10.23	108	3.16×10^8	8.11×10^{10}
	256	2.19×10^8	8.00×10^{10}
	500	2.11×10^8	7.87×10^{10}
9.25	108	2.31×10^8	8.60×10^{10}
	256	3.41×10^8	8.50×10^{10}
	500	3.18×10^8	8.36×10^{10}
8.12	108	2.45×10^8	9.18×10^{10}
	256	4.31×10^8	9.06×10^{10}
	500	3.38×10^8	8.91×10^{10}
7.15	108	3.52×10^8	9.80×10^{10}
	256	3.00×10^8	9.69×10^{10}
	500	4.08×10^8	9.55×10^{10}
6.17	108	3.39×10^8	1.06×10^{11}
	256	2.28×10^8	1.05×10^{11}
	500	2.53×10^8	1.04×10^{11}

[a]The former is from eq 2, whereas the latter is from eq 22.

Table 4. Summary of the Zeldovich Factor Calculated by Eqs 11 and 12 in ref 23

	fitting			
S	108	256	500	approximation
10.23	0.215	0.215	0.205	0.134
9.25	0.164	0.170	0.209	0.128
8.12	0.160	0.175	0.149	0.121
7.15	0.133	0.168	0.123	0.114
6.17	0.163	0.153	0.196	0.105

in Figure 7, one can understand the source of the discrepancies portrayed in Figure 6a. The source of the orderly variation is in the forward rate f^*, as can be seen in Table 3, which has been documented to be interesting because other MD studies[30,32] find the exponential term to be the main source of difference. The declining trend will be explained later in the text.

The panels in Figure 7 are illustrations of the Gibbs free energy, calculated by the cluster formation free energy method, and CNT, which is calculated from

$$\Delta G(n) = \gamma(36\pi v_l^2)^{1/3} n^{2/3} - nk_B T \ln S \qquad (25)$$

The peaks from eq 25 coincide with that of the values calculated from eq 17. Though the free energy barrier is higher for lower S values, which coincides with the nucleation theory, no general tendency can be seen for the seed size. An interesting point is that there is no significant variation in the height of the peaks for the CNT results, unlike that from the formation free energy analysis. This is actually the source of the declining trend mentioned in Figure 6a. The exponential term in eq 19 does affect the homogeneous nucleation characteristics, but only to the extent of generating a two order difference between the highest and the lowest S values that were examined. Affecting the nucleation phenomena by two orders is quite modest when considering experimental results and CNT easily differ by 20 orders of magnitude.[51−54]

4.2. Critical Nucleus. Besides using the first nucleation theorem in eq 24, the critical nucleus can also be obtained from the cluster formation free energy analysis, CNT, and kinetic analysis, where the first two can be found from Figure 7. Figure

dx.doi.org/10.1021/jp3044658 | J. Phys. Chem. B 2012, 116, 14637−14649

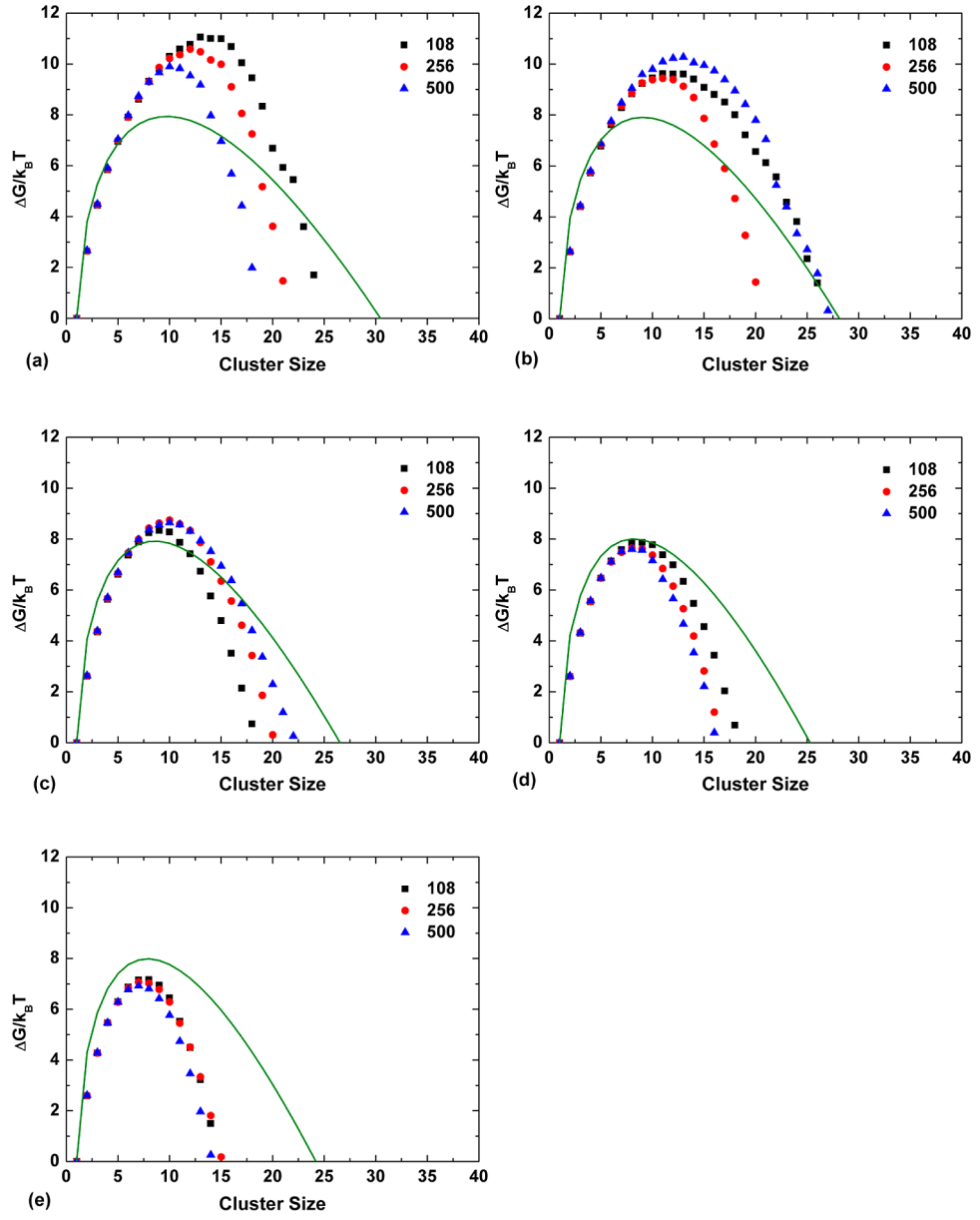

Figure 7. Gibbs free energy plot for the cubic seed for high supersaturation ratios: (a) $S = 6.17$, (b) 7.15, (c) 8.12, (d) 9.25, and (e) 10.23. The free energy barrier is clearly lower for a higher S value, which coincides with the classical nucleation theory. The solid line is from CNT for each representative supersaturation ratio calculated from eq 25.

8 shows the results from the three methods. Figure 8a is from the free energy analysis method, which is basically extracting information from the MD results. Above critical S, the lower supersaturation ratio generally has a larger critical nucleus size, which means more free energy is required for nucleation to persist. The comparison of the data is Figure 8a and CNT is Figure 8b, where the better the two agree, the closer the data points will be on the dashed line. Averages for the values at each S were used for the formation free energy to plot Figure 8b to clarify the trend. CNT shows a slight underestimation for the critical nucleus size, which coincides with the spherical seed. Kinetic analysis in Figure 8c shows the worst agreement, which is commonly observed in other MD studies.[23,31] Note that the critical nucleus size from the first nucleation theorem, which was 7.877, is similar to the value for high supersaturation ratios. Coupled with what has been learned from the nucleation rates, one must believe it is safe to say that the homogeneous nucleation characteristics are not affected by the seed size or shape.

4.3. Nanoparticle Growth. The growth rate, which is defined as the number of molecules that attach to the surface of the initial wetted seed particle per unit time per unit surface area, is depicted in Figure 9. A seed size dependence is evident, where a smaller seed actually has a higher growth rate, but more interestingly, there is no clear supersaturation ratio dependence, which is expected based on CNT.[34]

The logarithmic plot in Figure 10 produces a near zero slope, which implies that the critical nucleus size is a negative value. This can be understood as the seed particle being over the critical value, and growth can occur spontaneously. The slope is greater than that of the spherical seed, which was 9.3×10^{-3}, but does not have any significant meaning unless it is greater than 1.0.

dx.doi.org/10.1021/jp3044658 | J. Phys. Chem. B 2012, 116, 14637−14649

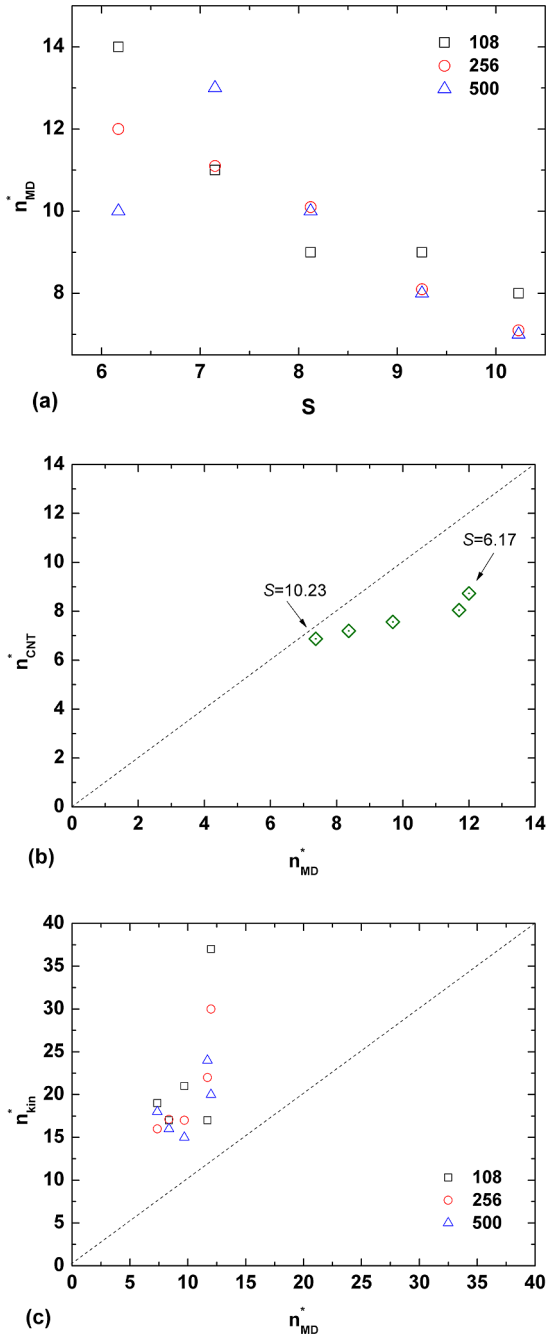

Figure 8. (a) Critical nucleus size (n^*_{MD}) from the cluster formation free energy method. (b) Comparison of the critical nucleus size for CNT and n^*_{MD}. (c) Comparison of the critical nucleus size for kinetic analysis and n^*_{MD}. Closer to the dashed line means better agreement between both methods.

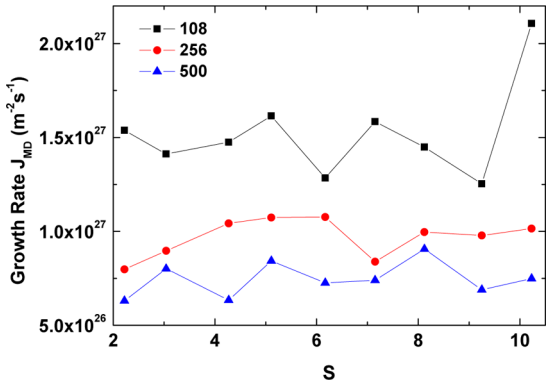

Figure 9. Growth rate plot for all three seed sizes. Though a seed size dependence can be seen, the supersaturation ratio seems to have no affect on the growth rate. The connecting lines are placed to simply guide the eye.

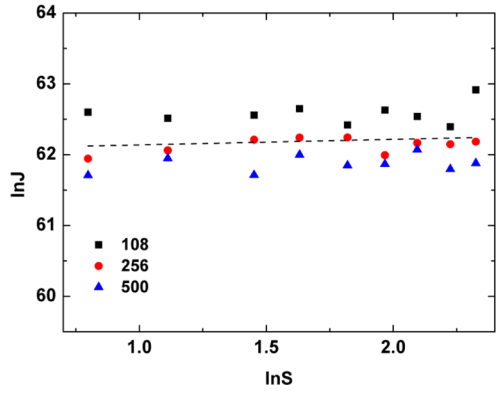

Figure 10. Natural log plot for the growth rate and supersaturation ratio. The slope from the linear fit (dashed line) is 0.0784, which implies that the seed is larger than the critical nucleus size, and spontaneous growth occurs.

Table 5. Nondimensionalized Monolayer Thickness (σ_{Al}) of All Seeds for All Supersaturation Ratios

	seed type		
S	108	256	500
10.23	1.08	1.08	1.08
9.25	1.08	1.09	1.08
8.12	1.08	1.07	1.08
7.15	1.07	1.08	1.09
6.17	1.07	1.08	1.08
5.11	1.08	1.08	1.09
4.27	1.07	1.08	1.08
3.03	1.07	1.08	1.08
2.22	1.08	1.08	1.09

The classical nucleation theory for growth on a cubic seed was explained in section 2. The only parameter that needs further explanation is the monolayer thickness, which is presented in Table 5. A new method was developed to calculate the distance between the molecules on the seed surface and the wetted vapor molecules. First, molecules on the surface of the seed were distinguished as vertex, edge, and face molecules. Second, the vapor molecules neighboring the molecules on the faces were classified for each surface. Third, three molecules in the same face were selected to generate an equation of a plane. Finally, the distance between the plane and each vapor molecule was calculated and averaged for all faces.

All combinations for selecting three molecules in the same face were examined, but through trial-and-error, we have found that two criteria are necessary. The first is that the three points cannot be in a straight line, and the second is that all three points require a sufficient distance between each other in order to level out the tilt of the plane that may occur when the three points that are selected are far from the vapor molecule of interest. Therefore, initially, all combinations of planes and corresponding vapor molecules were investigated, but only a

dx.doi.org/10.1021/jp3044658 | J. Phys. Chem. B 2012, 116, 14637−14649

fraction were actually used, and the averaging basically gave a more than reasonable result. As the seed size increases, there are obviously more combinations to be handled. The results in Table 5 show that the monolayer thickness is independent of seed size or supersaturation ratio. In addition, Table 6 presents the edge length that was used in the condensation theory.

Table 6. Nondimensionalized Edge Lengths (σ_{Al}) of the Cubic Seeds for All Supersaturation Ratios To Compare with Monolayer Thicknesses in Table 5

	seed type		
S	108	256	500
10.23	6.33	8.99	11.67
9.25	6.32	8.97	11.65
8.12	6.32	8.99	11.66
7.15	6.31	8.99	11.67
6.17	6.32	8.99	11.66
5.11	6.33	8.99	11.66
4.27	6.33	9.00	11.66
3.03	6.33	9.00	11.67
2.22	6.32	8.99	11.66

The results in Figure 11 compared with that of MD show that while the seed size dependence is conserved, an S dependence emerges. Compared to the results for the sphere based on Fletcher,[34] the overall tendency for CNT in Figure 11a is similar, and the degree of orderly deviation is also comparable to ref 23. For the lowest supersaturation ratio and smallest seed size, the classical theory showed reasonable agreement. The MD results compared with the condensation theory in Figure 11b again show the overall tendency to be similar for the spherical seed.[23] The seed size dependence can be replicated by the condensation theory as well, but a different ascending tendency and overestimation is witnessed when compared with CNT.

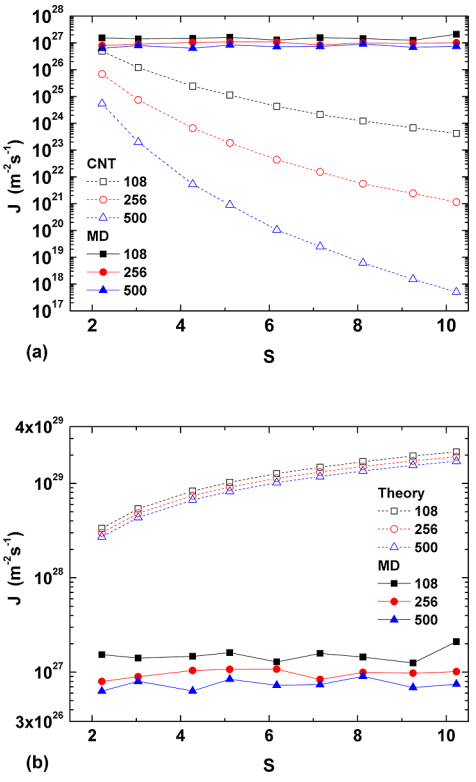

Figure 11. Growth rate from the simulation (MD) compared with (a) the classical nucleation theory and (b) condensation theory.

Figure 12 is the direct comparison of the growth rates between the cubic and the spherical seed, showing a 3−10 times faster growth rate for the cube regardless of S and the seed type. This is interesting because, even though the number of molecules within the seeds is nearly alike, the change in shape seems to have an effect on the growth characteristics. This is clearly evidence of a shape effect in growth. Moreover, the shape effect does not show a clear seed size dependence nor a S dependence.

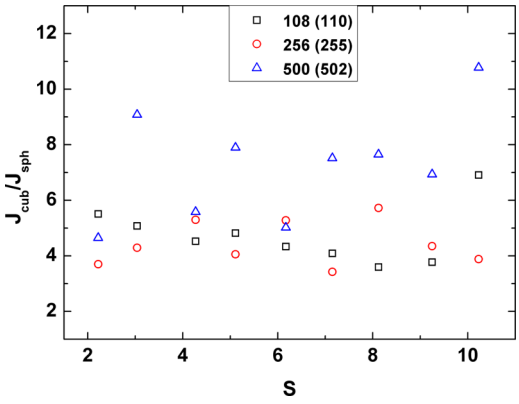

Figure 12. Plot for growth rate comparison between cubic and spherical seed. The cubic seed has an overall higher growth rate compared to the sphere, which is evidence of a shape effect. The shape effect does not show a clear seed size dependence nor an S dependence.

4.4. Growth Mechanism Analysis. To find the source of this shape effect, the potential energy generated solely from the interactions between the argon (vapor) and aluminum (seed) molecules were isolated and plotted in Figure 13. A lower and negative potential energy represents a stronger attraction. The surfaces on the cubic seed have a stronger attraction, which means attachment of vapor molecules occurs on the surfaces; moreover, this attachment is more widely distributed in comparison with the spherical seed.

To confirm why the cubic seed draws more vapor, a simple numerical analysis of a mesh of uniformly distributed simple cubic lattice points was set up. Each mesh point had a potential energy value that was consistent with argon LJ parameters. At the center of the cubic system of meshes, however, a volumetric region of the LJ parameters was changed to aluminum. The volumetric regions were lattice points that associated with either a sphere or cube, where the sphere had a diameter of 20, and the cube had an edge length of approximately 14 to synchronize the surface areas. The potential energy of the lattice point interactions between those that only had argon and aluminum interactions was calculated. The rough distribution for the sphere in Figure 14 is from a spherical cutting of the simple cubic lattice distributions. The overall tendencies for the simulation results in Figure 13 and the numerical results in Figure 14 qualitatively agree.

From Figures 13 and 14, one can deduce the source of the edge effect is actually not based on the presence of an edge, but due to a lack of a curvature,[55,56] which is distinctly different from crystal growth.[57] As can be seen in the previous plots, for

dx.doi.org/10.1021/jp3044658 | J. Phys. Chem. B 2012, 116, 14637−14649

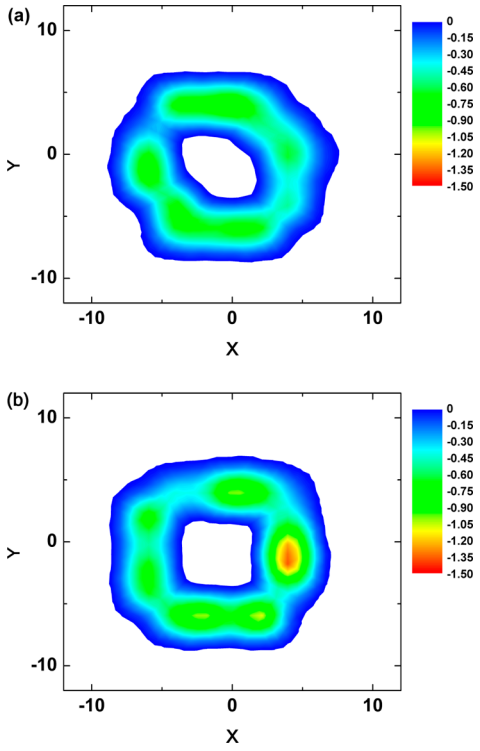

Figure 13. Potential energy contour plots from MD. Only the interactions between vapor and seed molecules for the (a) spherical and (b) cubic seed were illustrated. These are slice plots of one replication for the largest seed at S = 2.22 at 100 ps.

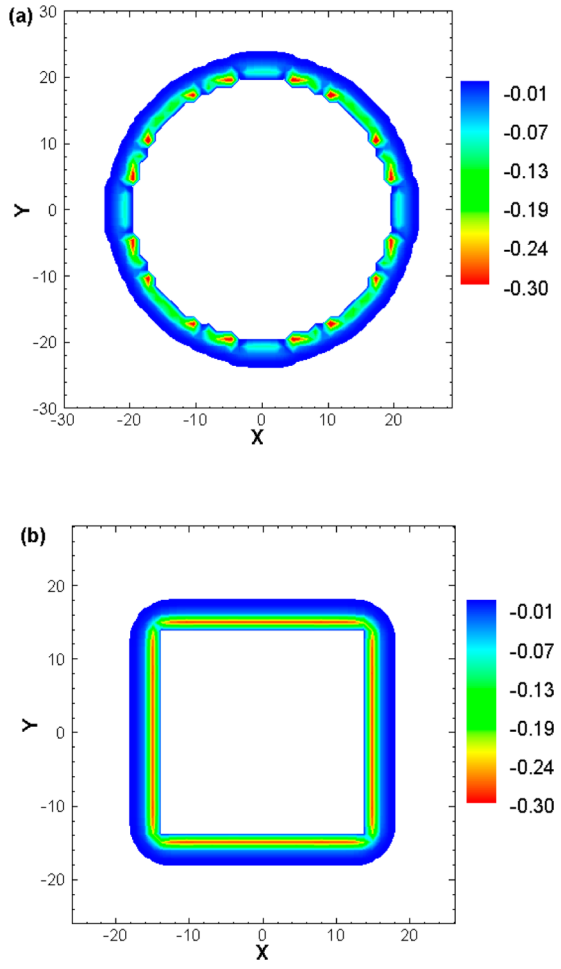

Figure 14. Numerical analysis of the potential energy between argon and aluminum lattice points for (a) spherical and (b) cubic seed shapes.

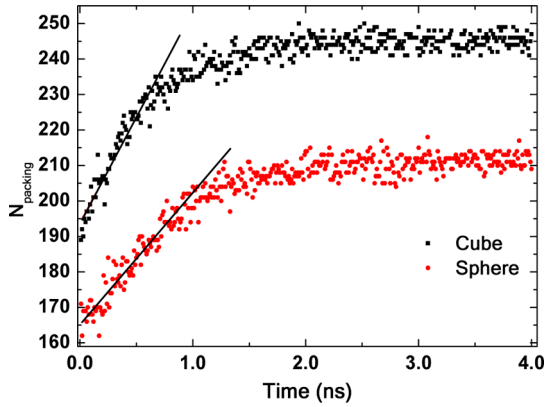

Figure 15. Evolution of packing of molecules adjacent to the largest seed for one replication at S = 2.22. The lines are linear fits with slopes of 0.589 for the cube and 0.372 for the sphere, which are the packing rates for each shape.

vapor condensation, the edge does not induce growth, but is simply a geometric byproduct. Vapor actually gathers on the faces of the cubic seeds. From a macroscopic perspective, diffusion near the vapor−liquid interface of the growing particle is relatively fast compared to the diffusion between the particle and the ambient system, so a curved surface will effectively increase the saturation pressure, $P_{sat}(T)$, and thus relatively decrease the local supersaturation ratio, S_{local}, for the spherical seed.[58] This is consistent with the Kelvin effect.[59]

As stated earlier, condensation commences from complete wetting (zero contact angle) on the FCC seed, but packing of molecules onto the seed surface continues well after the initiation (Figure 15). The slopes of the two shapes are only of the first layer on the seed, so their values divided by the aforementioned surface areas are different from the actual growth rates in Figure 12. The first layer was defined as vapor molecules that have at least one neighboring seed molecule within a distance of $1.4\sigma_{Al}$. Though the monolayer thickness is less than this value (Table 5), it produces a correct list of molecules based on the Pythagorean theorem applied for three dimensions. Additionally, the second layer molecules are molecules that have first layer molecules as neighbors but no seed molecule neighbors with also a cutoff of $1.4\sigma_{Al}$.

The packing number $N_{packing}$ in Figure 15 saturates between 2.0−4.0 ns for both shapes, so the average value taken within this time frame will be called the "saturated packing number." The initial packing number is defined as the average packing number of the first 10 data points. The saturated packing number for the sphere and cube are 210.8 and 245.0, respectively. Additionally, the initial packing numbers are 168.8 and 195.2, so the level of packing is the initial packing number divided by the saturated packing number, which becomes 0.801 and 0.797 for the sphere and cube, respectively. The simple difference between the initial and saturated packing number for the sphere and cube are Δn_s = 42.0 and Δn_c = 49.8, respectively. The higher packing rate and Δn_c value on the cubic seed is another piece of evidence of a faster growth rate. The minute difference in the level of packing suggests the level of packing is initially the same regardless of seed shape. The

dx.doi.org/10.1021/jp3044658 | J. Phys. Chem. B 2012, 116, 14637−14649

number of potential lattice sites to be filled, however, is innately different for seed shape, and they are eventually filled at a different pace. This is interesting coupled with the fact that the initial surface area of the sphere is actually slightly greater than the cube (Table 1). Thus, the conclusion that a flat surface with a lattice structure has a stronger influence on vapor molecules near the surface can be drawn.

Further analysis on the packing characteristics is studied by observing the surface diffusion (namely, detachment and hopping) of the molecules in the first layer on the seed, which is prominent in phase transitions (Figure 16).[60] A detachment event is defined as a vapor molecule that was in the first layer at one time step and not being in the first layer at the next time step. Moreover, a hopping event is when a vapor molecule in the first layer at a time step changes its lattice position (has different neighboring seed molecules) at the next time step. Generally, the amount of diffusion decreases as packing increases as in the previous figure, which is physically comprehensible because more molecules attaching on the seed surface and outer regions of the growing particle makes the molecules close to the seed relatively crowded, and crowded molecules should have more difficulty in relocating. The interesting fact is that overall surface diffusion never goes to zero.

Moreover, the panels in Figure 16 show that the spherical seed has more overall diffusion than the cube for both detachment of surface molecules and hopping within the first layer on the wetted surface. The rate of decrease for both events seems similar, but the latter has much more variation. Fewer detachment events for the cube suggest another reason for more growth, and this difference will no doubt dictate the growth on subsequent layers. This also signifies the fact that when considering condensation, the detachment rate can be just as important as the attachment rate of molecules.

Figure 17 is an example of how the vapor molecules exist on the cube surface. In order to confirm the persistence of the initial FCC structure of the seed and how it affects the first layer, Voronoi analysis was conducted.[61,62] Though the seed keeps its initial lattice structure, the first layer does not directly follow the FCC structure; however, the perception of epitaxial growth cannot be completely abandoned because more than a few vapor molecules conform to the voids on the surface, where solid molecules would exist. This loose epitaxial growth makes the next layer and beyond become more disordered and thus can be fully designated as liquid. After the second layer is established, the growth mode changes from layer growth to formation of islands, which is also known as the Stranski-Krastanov growth mode for thin films.[63] On the other hand, growth on the spherical seed is more disordered and should be characterized as liquid starting from the first layer because the initial configuration is not a perfect sphere. Finally, unlike the assumptions of many numerical models, growth on nanoparticles is actually asymmetric (or nonisotropic) for both spherical and cubic seeds, and the cubic seed eventually becomes immersed inside a spherical liquid droplet.

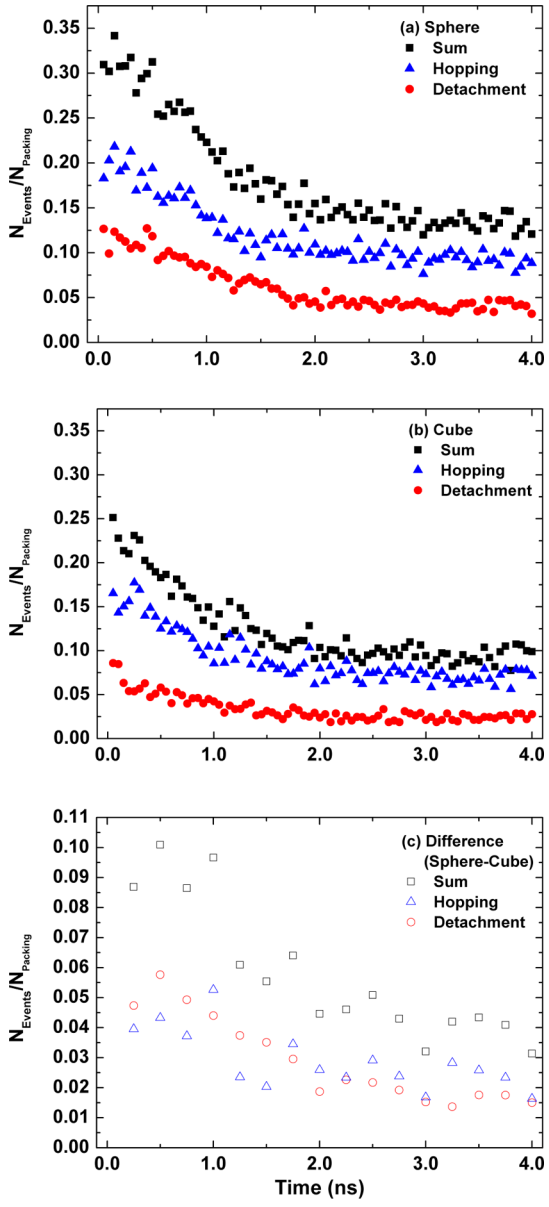

Figure 16. Time averaged number of surface diffusion events over the packing number in the first layer on the spherical and cubic seed surfaces, and the difference between the two shapes for one replication of seed size 500 at $S = 2.22$. "Sum" is the sum for both hopping and detachment events. More data points were averaged in (c) for better visualization.

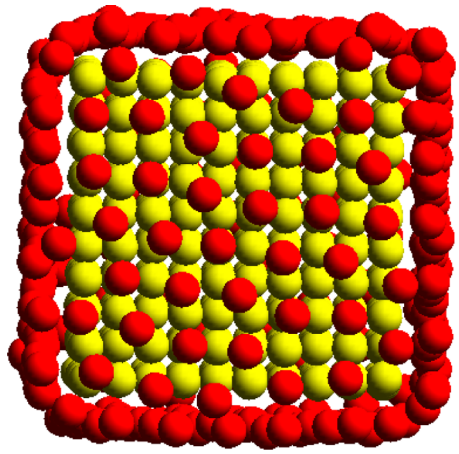

Figure 17. Snapshot of the first layer at 4.0 ns and evidence of a loose epitaxial growth on the cubic seed particle surface. Yellow and red are each the seed and vapor molecules, respectively.

dx.doi.org/10.1021/jp3044658 | J. Phys. Chem. B 2012, 116, 14637−14649

5. CONCLUSION

Nanoparticle growth on a cubic seed was studied by classical molecular dynamics simulation. The results were compared with a study on a set of systems containing a spherical seed. The two-stage phenomenon was observed once more, so heterogeneous growth and homogeneous nucleation were examined separately, and the results were compared to that from the spherical seed. Most tendencies were nearly identical to those from the spherical seed studies except for the nucleation rate being slightly higher for the sphere at lower supersaturation ratios. The heterogeneous growth rate was greater by a factor of 3 to 10, even though the number of molecules in each seed class was nearly identical, which was clear evidence of a shape effect. Cluster formation free energy analysis presented the free energy barrier for homogeneous nucleation and the resulting tendencies showed little to no difference.

A shape effect causes the difference in the growth mechanism, which has been verified by MD and numerical analysis to be that the curvature of the seed surface is the source. The packing and surface diffusion characteristics of the first layer offer very interesting insight into nanoparticle growth, bringing significance to the contributions of detachment of molecules.

AUTHOR INFORMATION

Corresponding Author

*E-mail: yasuoka@mech.keio.ac.jp.

Notes

The authors declare no competing financial interest.

ACKNOWLEDGMENTS

This work was supported in part by Grant in Aid for Scientific Research (Grant Nos. 20560198 and 24-6049) and the Global Center of Excellence Program for "Center for Education and Research of Symbiotic, Safe and Secure System Design" from the Ministry of Education, Culture, Sports, Science and Technology in Japan.

REFERENCES

(1) Koehler, K. A.; DeMott, P. J.; Kreidenweis, S. M.; Popovicheva, O. B.; Petters, M. D.; Carrico, C. M.; Kireeva, E. D.; Khokhlova, T. D.; Shonija, N. K. *Phys. Chem. Chem. Phys.* **2009**, *11*, 7906.
(2) Encrenaz, T. *Astron. Astrophys. Rev.* **1999**, *9*, 171.
(3) Rothen-Rutishauser, B. *Environ. Sci. Technol.* **2009**, *43*, 2634.
(4) Kulmala, M.; Riipinen, I.; Sipila, M.; Manninen, H. E.; Petaja, T.; Junninen, H.; Dal Maso, M.; Mordas, G.; Mirme, A.; Vana, M.; Hirsikko, A.; Laakso, L.; Harrison, R. M.; Hanson, I.; Leung, C.; Lehtinen, K. E. J.; Kerminen, V. M. *Science* **2007**, *318*, 89.
(5) Shafahi, M.; Bianco, V.; Vafai, K.; Manca, O. *Int. J. Heat Mass Transfer* **2010**, *53*, 376.
(6) Winkler, G.; Schnerr, G. H. *Z. Angew. Math. Mechanik* **2000**, *80*, S735.
(7) Altman, I. S.; Agranovski, I. E.; Choi, M. *Appl. Phys. Lett.* **2004**, *84*, 5130.
(8) Gorbunov, B. *J. Chem. Phys.* **1999**, *110*, 10035.
(9) Liu, X. Y. *J. Chem. Phys.* **1999**, *111*, 1628.
(10) Liu, X. Y. *J. Chem. Phys.* **2000**, *112*, 9949.
(11) Vehkamaki, H.; Maattanen, A.; Lauri, A.; Kulmala, M.; Winkler, P.; Vrtala, A.; Wagner, P. E. *J. Chem. Phys.* **2007**, *126*, 174707.
(12) Kuni, F. M.; Shchekin, A. K.; Grinin, A. P. *Uspekhi Fizicheskikh Nauk* **2001**, *171*, 345.
(13) Kuni, F. M.; Shchekin, A. K.; Rusanov, A. I.; Widom, B. *Adv. Colloid Interface Sci.* **1996**, *65*, 71.
(14) Berg, W. F. *Proc. R. Soc. A* **1938**, *164*, 0079.
(15) Hurle, D. T. J. *Handbook of Crystal Growth*; North-Holland: Amsterdam; New York, 1993.
(16) Markov, I. V. *Crystal Growth for Beginners: Fundamentals of Nucleation, Crystal Growth, And Epitaxy*; World Scientific: Singapore; New Jersey, 1995.
(17) Sunagawa, I. *Crystals: Growth, Morphology, And Perfection*; Cambridge University Press: Cambridge; New York, 2005.
(18) Winkler, P. M.; Steiner, G.; Vrtala, A.; Vehkamaki, H.; Noppel, M.; Lehtinen, K. E. J.; Reischl, G. P.; Wagner, P. E.; Kulmala, M. *Science* **2008**, *319*, 1374.
(19) Matsubara, H.; Ebisuzaki, T.; Yasuoka, K. *J. Chem. Phys.* **2009**, *130*, 104705.
(20) Walsh, M. R.; Koh, C. A.; Sloan, E. D.; Sum, A. K.; Wu, D. T. *Science* **2009**, *326*, 1095.
(21) Darvas, M.; Picaud, S.; Pal, J. *Phys. Chem. Chem. Phys.* **2011**, *13*, 19830.
(22) Inci, L.; Bowles, R. K. *J. Chem. Phys.* **2011**, *134*, 114505.
(23) Suh, D.; Yasuoka, K. *J. Phys. Chem. B* **2011**, *115*, 10631.
(24) Gaio, M.; Silvestrelli, P. L. *Phys. Rev. B* **2009**, *79*, 012102.
(25) Okazaki, K.; Sakuma, J.; Yasui, J.; Kuwabata, S.; Hirahara, K.; Tanaka, N.; Torimoto, T. *Chem. Lett. 40*, 84.
(26) Rut'kov, E. V.; Gall, N. R. *Phys. Solid State* **2009**, *51*, 1738.
(27) Ganapathy, R.; Buckley, M. R.; Gerbode, S. J.; Cohen, I. *Science* **2010**, *327*, 445.
(28) Carvalho, J. L.; Dalnoki-Veress, K. *Phys. Rev. Lett. 105*, 237801.
(29) Tang, C. J.; Fernandes, A. J. S.; Buijnsters, J. G.; Abe, I.; Domingues, M. F. F.; Pinto, J. L. *Phys. Status Solidi A* **2010**, *207*, 2029.
(30) Yasuoka, K.; Matsumoto, M. *J. Chem. Phys.* **1998**, *109*, 8451.
(31) Matsubara, H.; Koishi, T.; Ebisuzaki, T.; Yasuoka, K. *J. Chem. Phys.* **2007**, *127*, 214507.
(32) Yasuoka, K.; Matsumoto, M. *J. Chem. Phys.* **1998**, *109*, 8463.
(33) Fogler, H. S. *Elements of Chemical Reaction Engineering*, 4th ed.; Prentice Hall: Westford, MA, 2005.
(34) Fletcher, N. H. *J. Chem. Phys.* **1958**, *29*, 572.
(35) Kashchiev, D. *Nucleation: Basic Theory with Applications*, 1st ed.; Butterworth-Heinemann: New York, 2000.
(36) ter Horst, J. H.; Kashchiev, D. *J. Chem. Phys.* **2003**, *119*, 2241.
(37) Cai, J.; Ye, Y. Y. *Phys. Rev. B* **1996**, *54*, 8398.
(38) Hodak, J. H.; Henglein, A.; Hartland, G. V. *J. Chem. Phys.* **1999**, *111*, 8613.
(39) Murray, D. B.; Saviot, L. *Phys. E* **2005**, *26*, 417.
(40) Agrawal, P. M.; Rice, B. M.; Thompson, D. L. *Surf. Sci.* **2002**, *515*, 21.
(41) Holcomb, C. D.; Clancy, P.; Thompson, S. M.; Zollweg, J. A. *Fluid Phase Equilib.* **1992**, *75*, 185.
(42) Mecke, M.; Winkelmann, J.; Fischer, J. *J. Chem. Phys.* **1997**, *107*, 9264.
(43) Trokhymchuk, A.; Alejandre, J. *J. Chem. Phys.* **1999**, *111*, 8510.
(44) Linstrom, P. J.; Mallard, W. G. *NIST Chemistry WebBook, NIST Standard Reference Database Number 69*; National Institute of Standards and Technology: Gaithersburg, MD, 20899, 2010; http://webbook.nist.gov.
(45) Stillinger, F. H., Jr *J. Chem. Phys.* **1963**, *38*, 1486.
(46) Suh, D.; Yoon, W.; Shibahara, M.; Jung, S. *J. Chem. Phys.* **2008**, *128*, 154523.
(47) Kashchiev, D. *J. Chem. Phys.* **1982**, *76*, 5098.
(48) Thompson, S. M.; Gubbins, K. E.; Walton, J.; Chantry, R. A. R.; Rowlinson, J. S. *J. Chem. Phys.* **1984**, *81*, 530.
(49) Chapela, G. A.; Saville, G.; Thompson, S. M.; Rowlinson, J. S. *J. Chem. Soc., Faraday Trans. 2* **1977**, *73*, 1133.
(50) Wedekind, J.; Wolk, J.; Reguera, D.; Strey, R. *J. Chem. Phys.* **2007**, *127*, 154515.
(51) Iland, K.; Wolk, J.; Strey, R.; Kashchiev, D. *J. Chem. Phys.* **2007**, *127*, 154506.
(52) Sinha, S.; Bhabhe, A.; Laksmono, H.; Wolk, J.; Strey, R.; Wyslouzil, B. *J. Chem. Phys.* **2010**, *132*, 064304.
(53) Wedekind, J.; Chkonia, G.; Wolk, J.; Strey, R.; Reguera, D. *J. Chem. Phys.* **2009**, *131*, 114506.

(54) Iland, K.; Wedekind, J.; Wolk, J.; Strey, R. *J. Chem. Phys.* **2009**, *130*, 114508.
(55) Zeng, J.; Huang, J. L.; Liu, C.; Wu, C. H.; Lin, Y.; Wang, X. P.; Zhang, S. Y.; Hou, J. G.; Xia, Y. N. *Adv. Mater.* **2010**, *22*, 1936.
(56) Bai, X. M.; Li, M. *Nano Lett.* **2006**, *6*, 2284.
(57) Lao, J. Y.; Huang, J. Y.; Wang, D. Z.; Ren, Z. F. *Nano Lett.* **2003**, *3*, 235.
(58) Moody, M. P.; Attard, P. *Phys. Rev. Lett.* **2003**, *91*, 056104.
(59) Hinds, W. C. *Aerosol Technology: Properties, Behavior, and Measurement of Airborne Particles*, 2nd ed.; Wiley-Interscience: New York, 1999.
(60) Zhang, H. Z.; Banfield, J. F. *Nano Lett.* **2004**, *4*, 713.
(61) Tanemura, M.; Hiwatari, Y.; Matsuda, H.; Ogawa, T.; Ogita, N.; Ueda, A. *Prog. Theor. Phys.* **1977**, *58*, 1079.
(62) Finney, J. L. *J. Comput. Phys.* **1979**, *32*, 137.
(63) Grabow, M. H.; Gilmer, G. H. *Surf. Sci.* **1988**, *194*, 333.